Supporting Information

Imidazole-Functionalized Polyoxometalate Catalysts for the Oxidation of 5-Hydroxymethylfurfural to 2,5‑Diformylfuran Using Atmospheric O_2

Dan Liu,† Baokuan Chen,‡ Jie Li,† Zhengguo Lin,† Peihe Li,† Ni Zhen,† Yingnan Chi,*† and Changwen Hu*†*

† Key Laboratory of Cluster Science, Ministry of Education of China, School of Chemistry and Chemical Engineering, Beijing Institute of Technology, Beijing, 100081 P.R. China

‡ School of Petrochemical Engineering, Liaoning Shihua University, Fushun, Liaoning, 113001, P. R. China

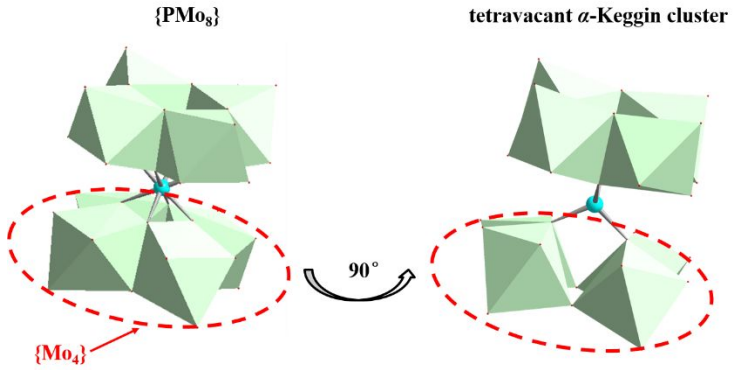

Figure S1. The structural relationship between the $\{PMo_8\}$ in our case and the tetravacant α-Keggin cluster.

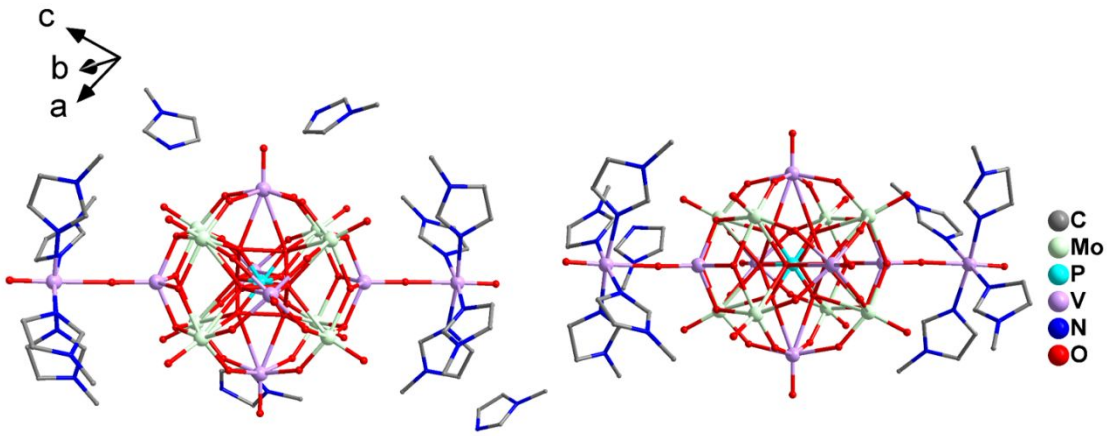

Figure S2. Cocrystallization of 1-methylimidazole and the imidazole-functionalized cluster.

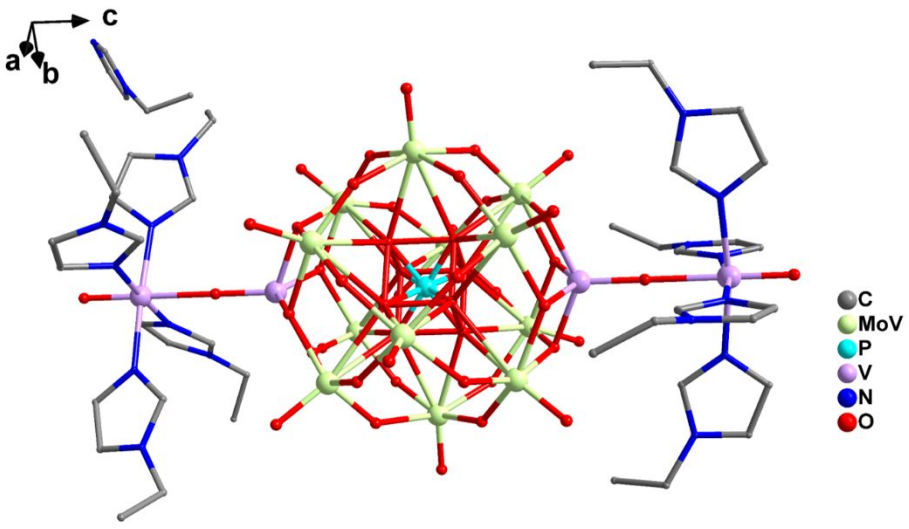

Figure S3. Cocrystallization of 1-ethylimidazole and the imidazole-functionalized cluster.

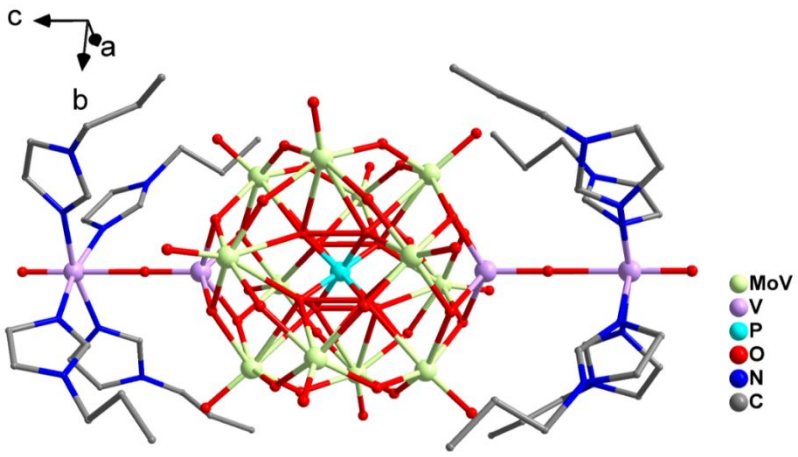

Figure S4. Cocrystallization of 1-propylimidazole and the imidazole-functionalized cluster.

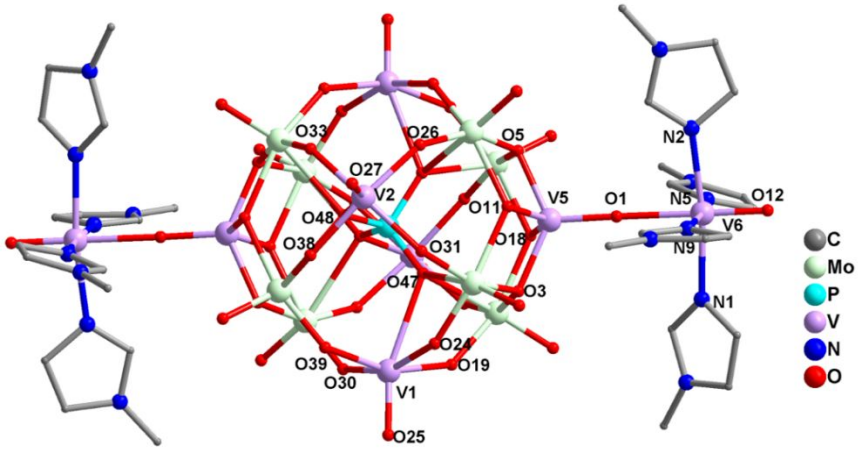

Figure S5. Ball-and-stick representation of compound **1**.

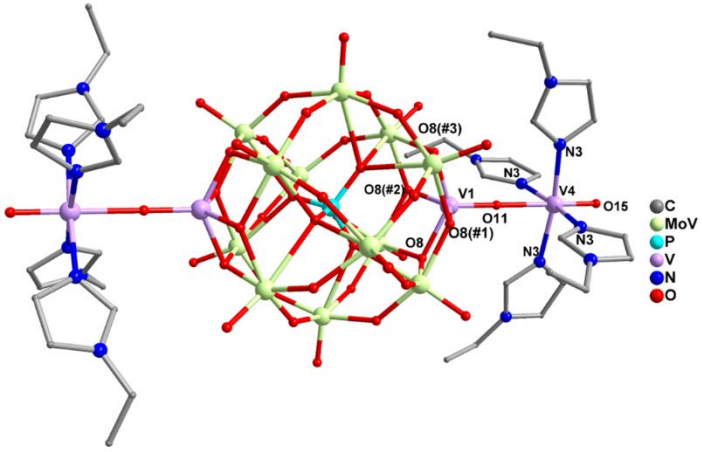

Figure S6. Ball-and-stick representation of compound **2**.

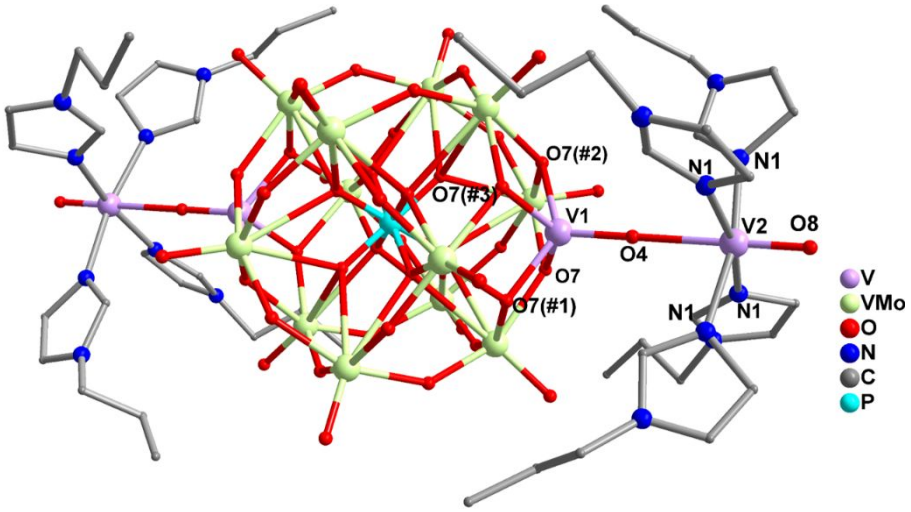

Figure S7. Ball-and-stick representation of compound **3**.

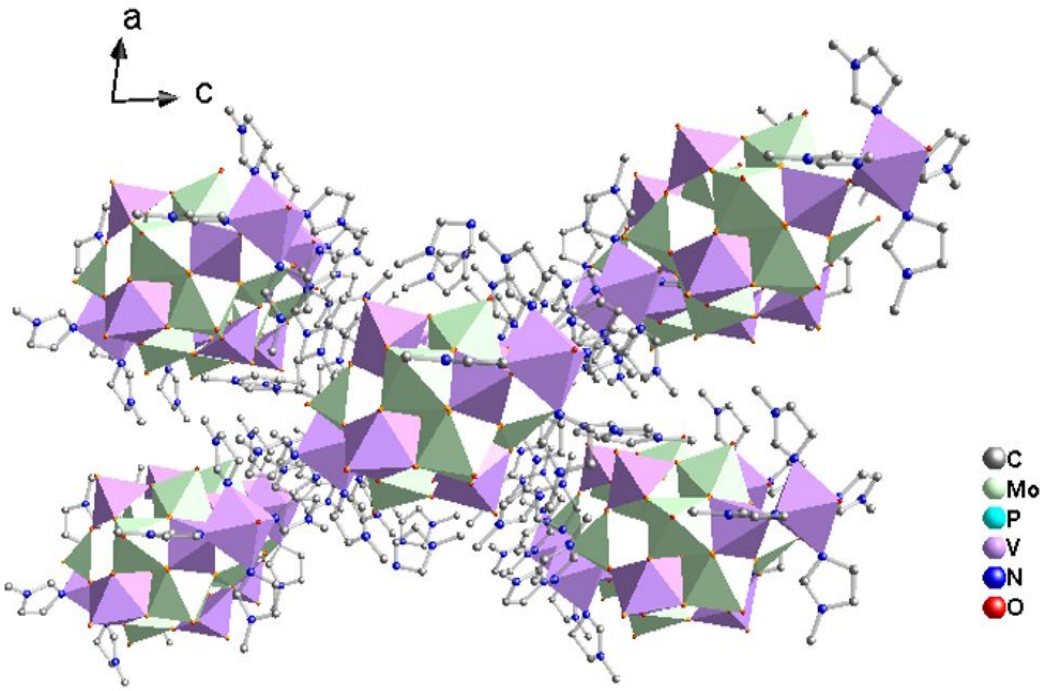

Figure S8. The packing view of compound **1** along *b* axis.

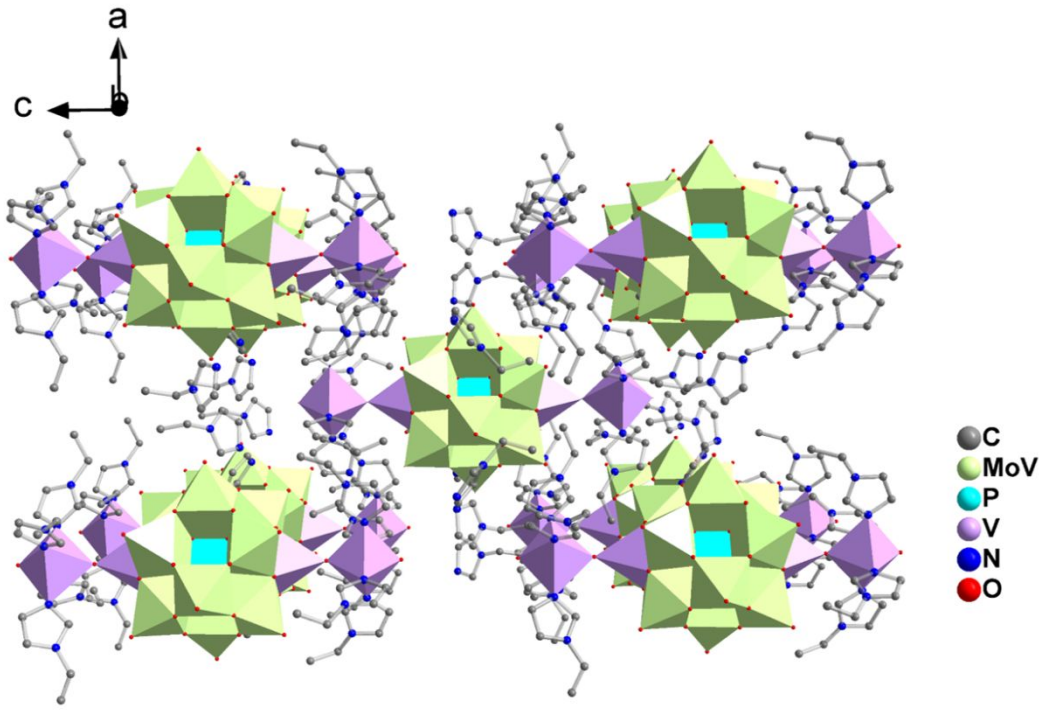

Figure S9. The packing view of compound **2** along *b* axis.

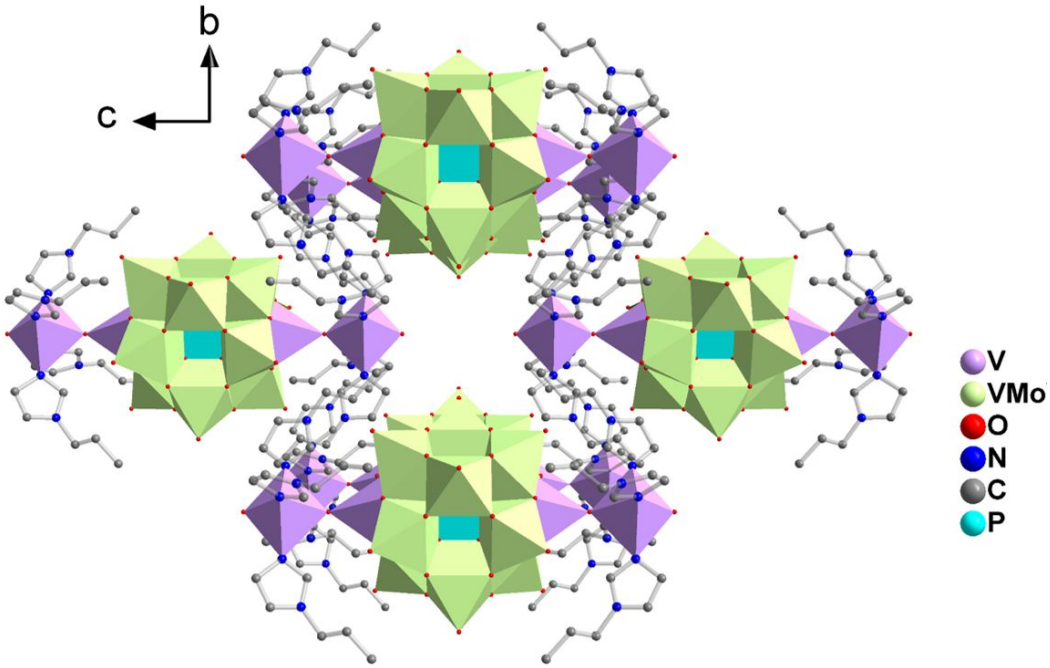

Figure S10. The packing view of compound **3** along *a* axis.

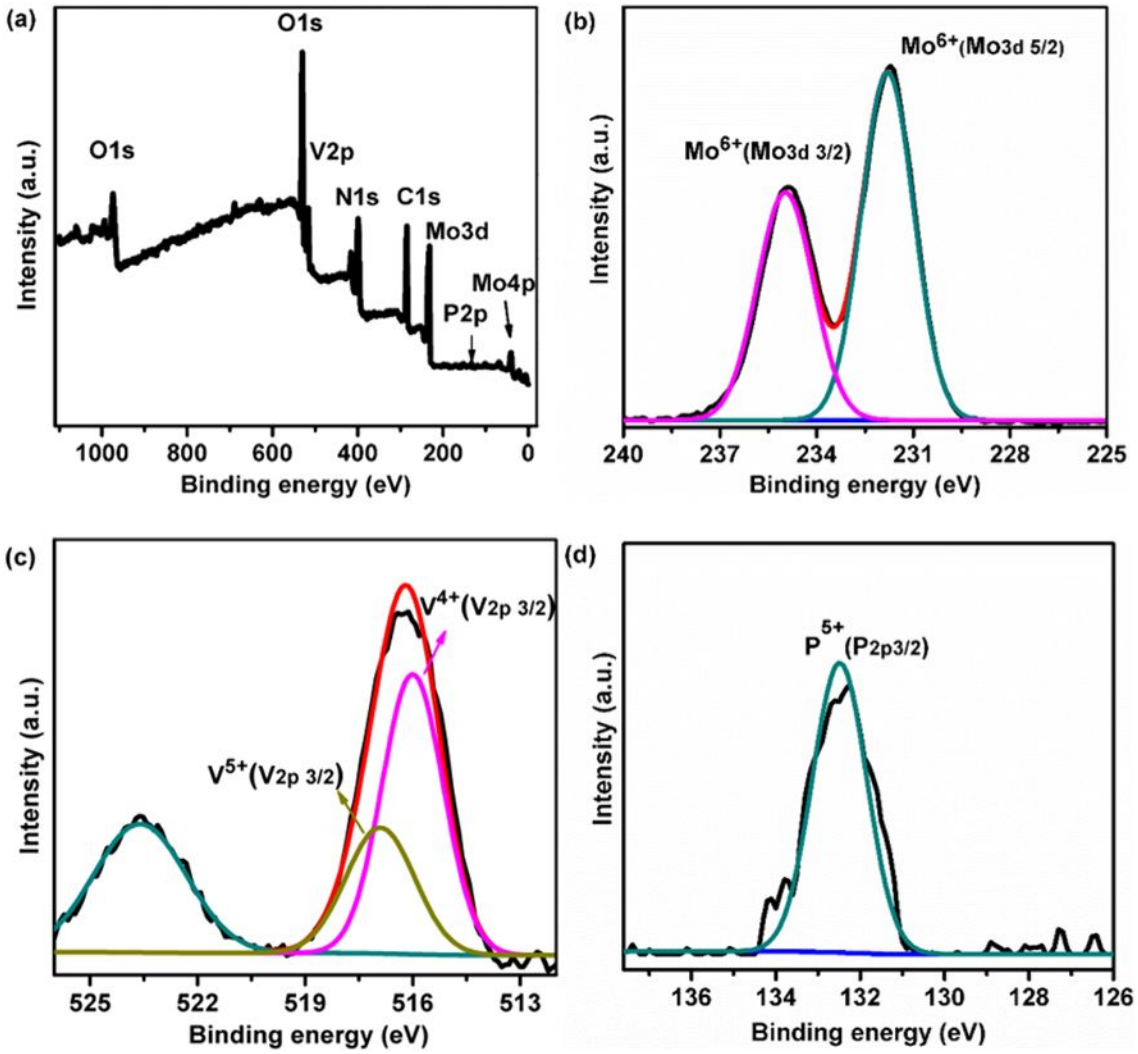

Figure S11. XPS curves of compound **1**. (a) survey spectra of compound **1**; (b) Mo 3d spectra of compound **1**; (c) V 2p spectra of compound **1**; (d) P 2p spectra of compound **1**.

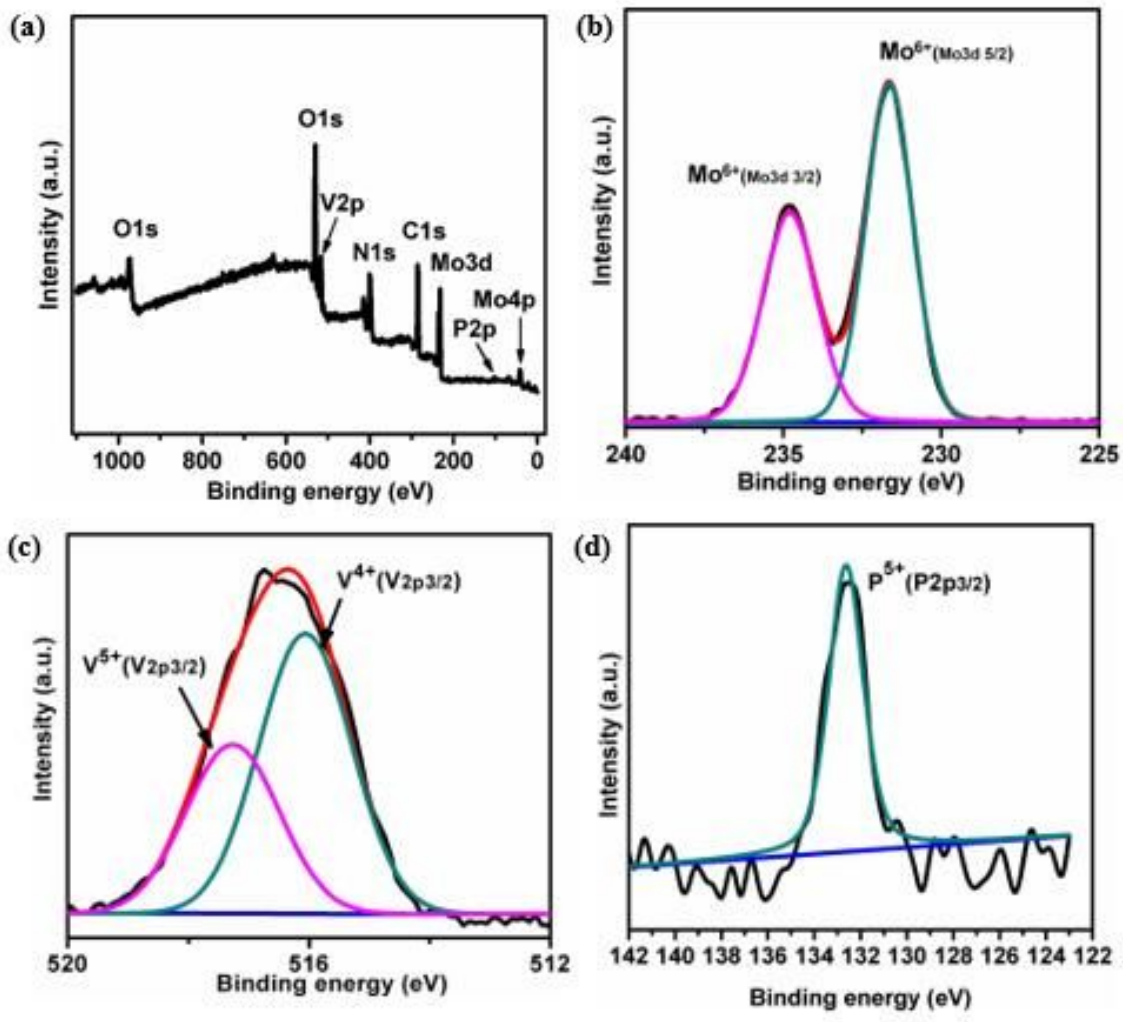

Figure S12. XPS curves of compound **2**. (a) survey spectra of compound **2**; (b) Mo 3d spectra of compound **2**; (c) V 2p spectra of compound **2**; (d) P 2p spectra of compound **2**.

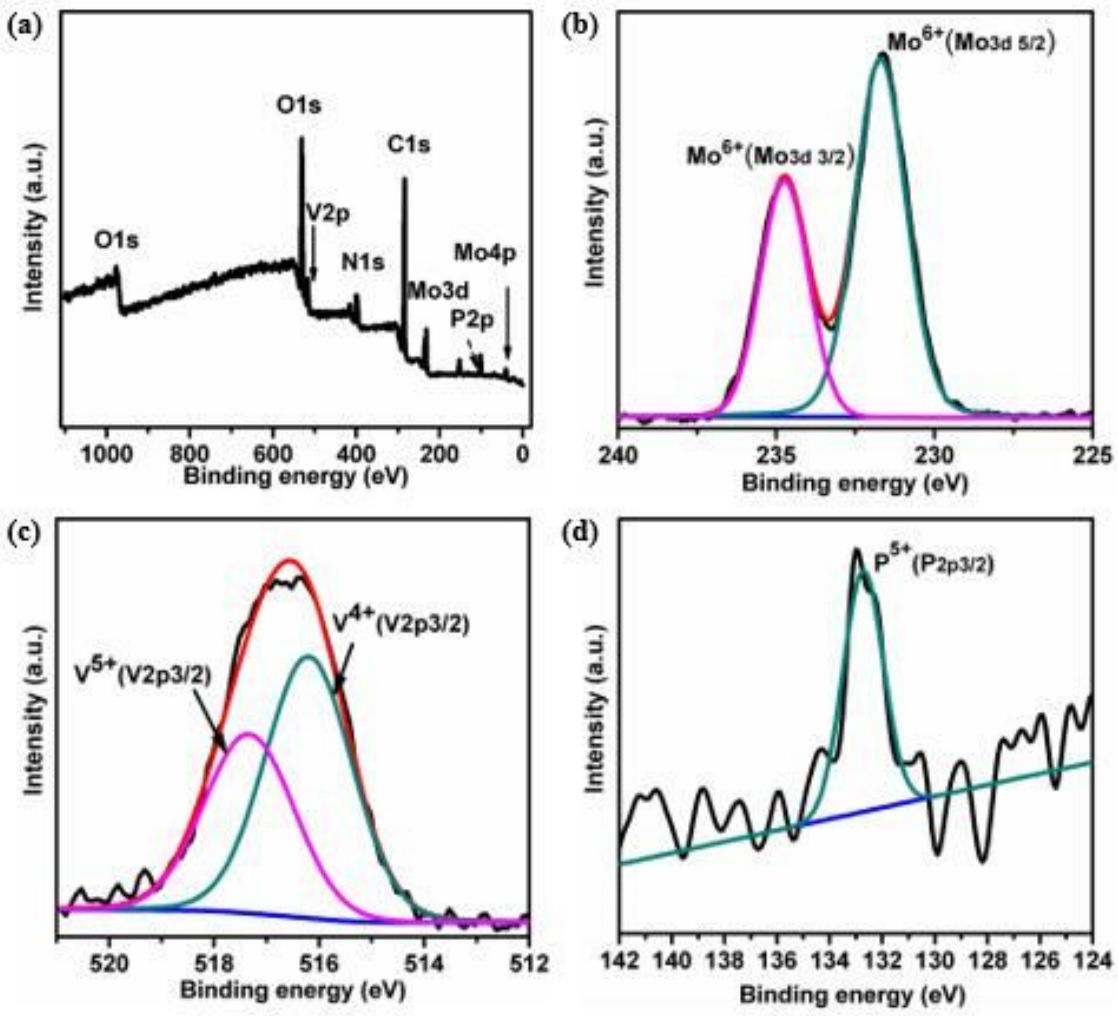

Figure S13. XPS curves of compound **3**. (a) survey spectra of compound **3**; (b) Mo 3d spectra of compound **3**; (c) V 2p spectra of compound **3**; (d) P 2p spectra of compound **3**.

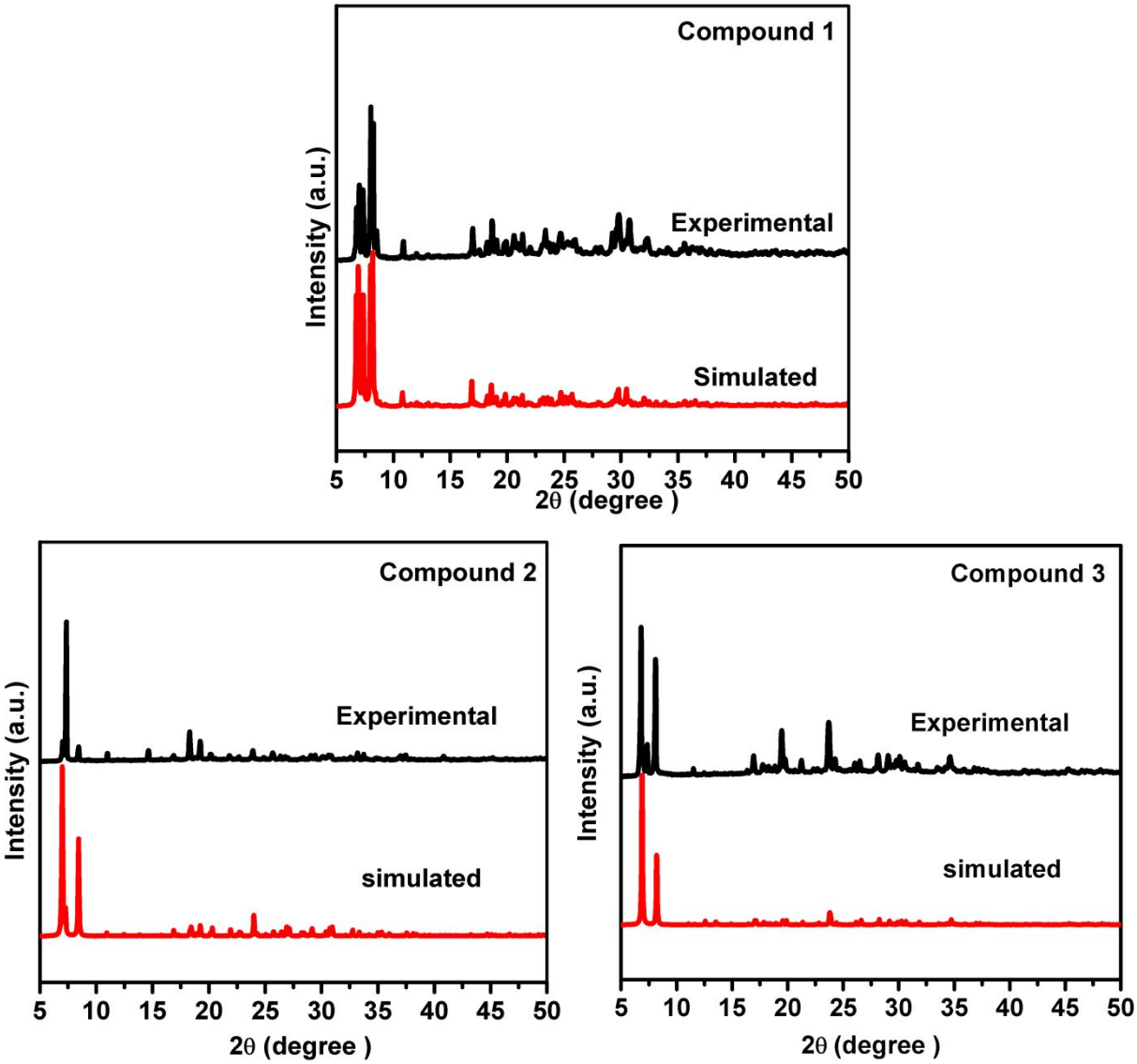

Figure S14. Experimental and simulated XRD patterns of compounds **1-3**.

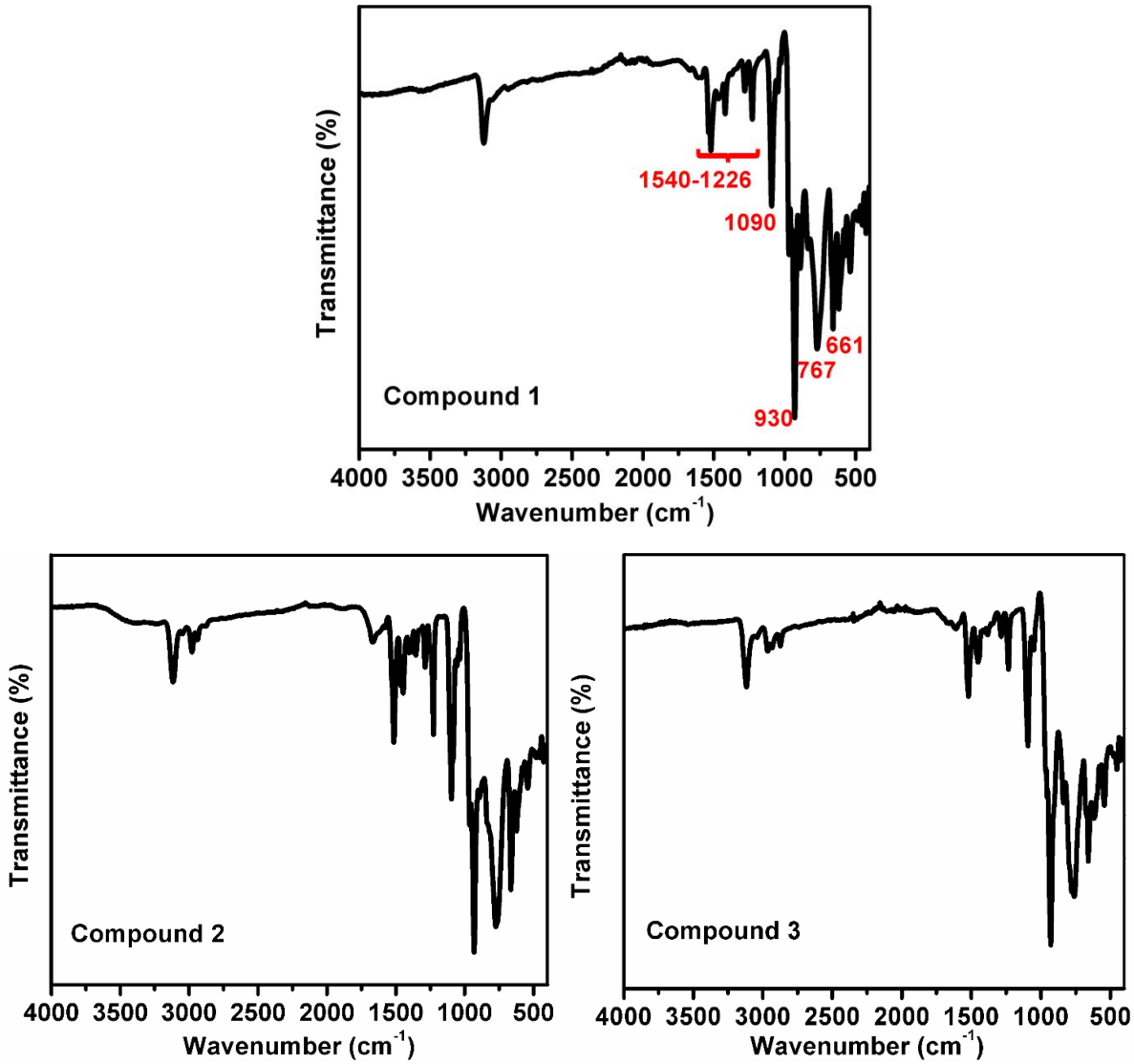

Figure S15. IR spectra of compounds **1-3**.

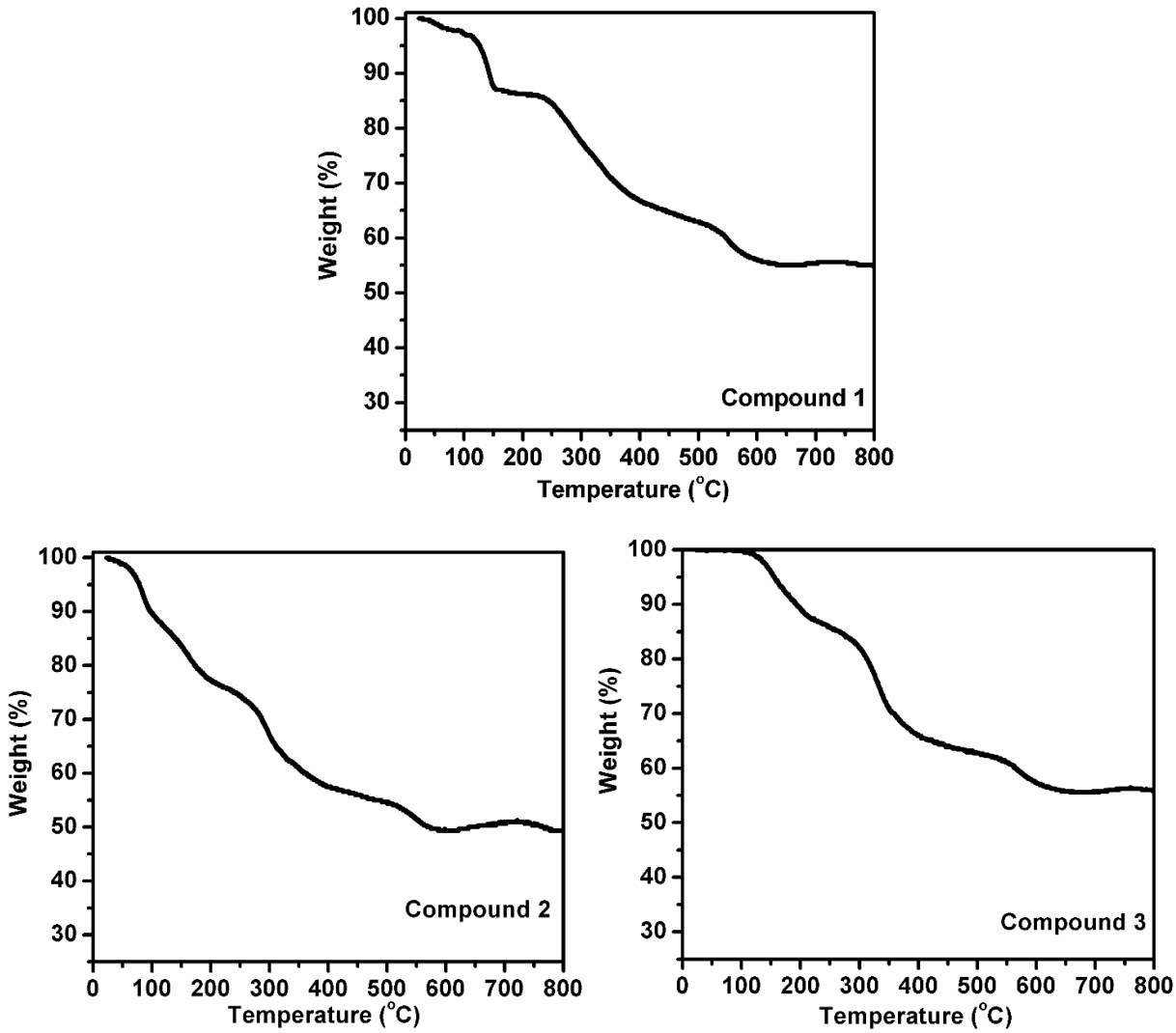

Figure S16. TGA curves of compounds **1-3**.

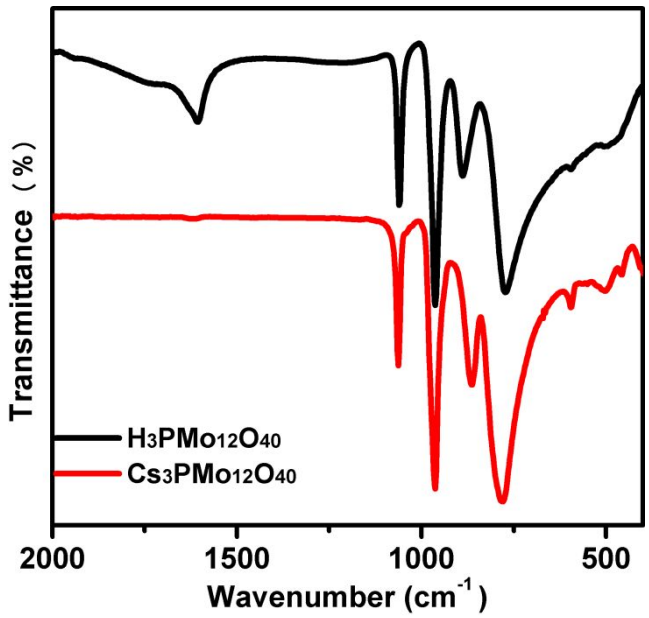

Figure S17. IR spectra of $Cs_3PMo_{12}O_{40}$ and $H_3PMo_{12}O_{40}$.

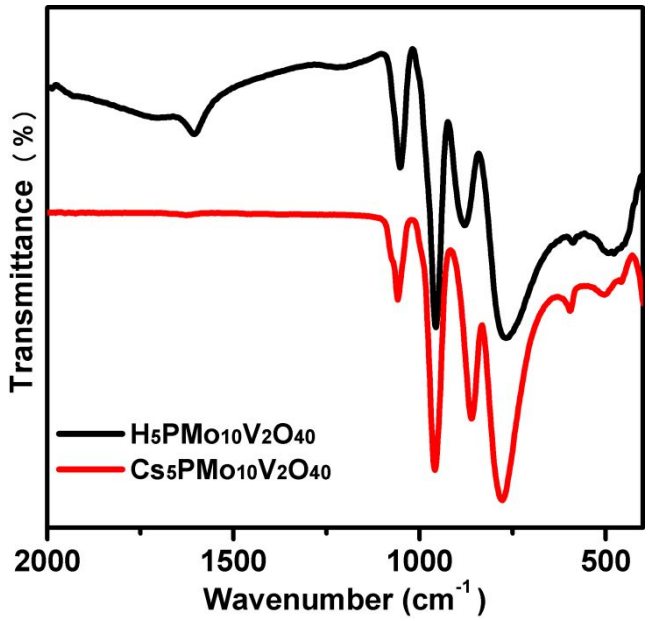

Figure S18. IR spectra of $Cs_5PMo_{10}V_2O_{40}$ and $H_5PMo_{10}V_2O_{40}$.

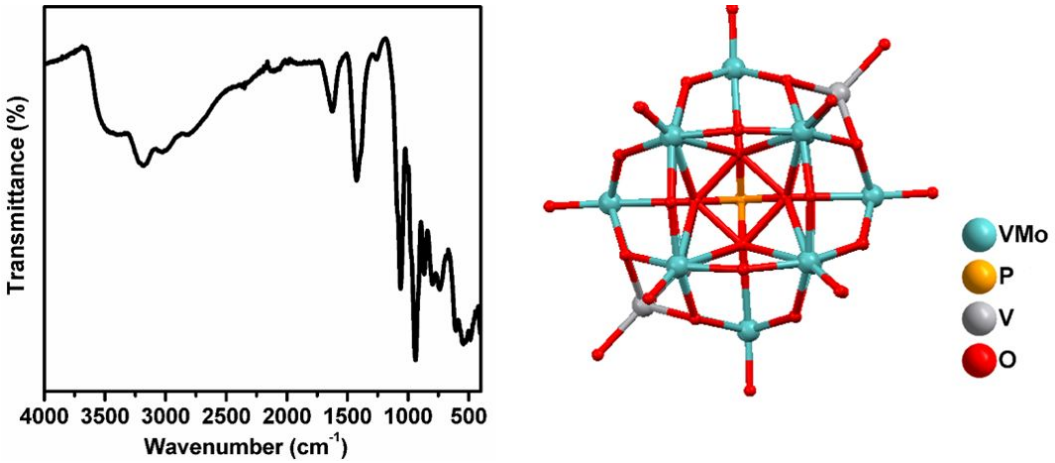

Figure S19. IR spectrum and ball-and-stick representation of $[NH_4]_4[HPMo_8V^{IV}{}_4O_{40}(V^{V}O)_2]$.

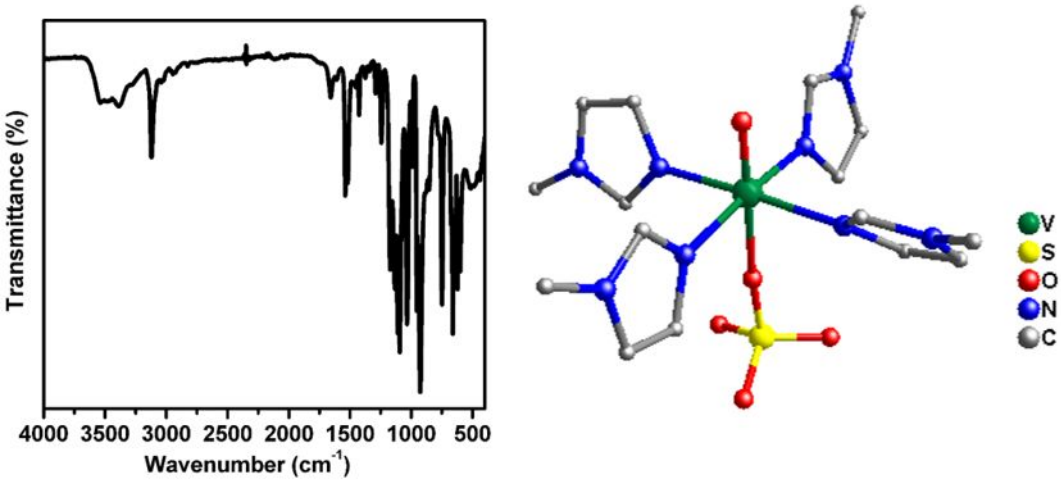

Figure S20. IR spectrum and ball-and-stick representation of $(V^{IV}O)(mIM)_4SO_4$.

Catalytic Experimental Section of HMF to DFF

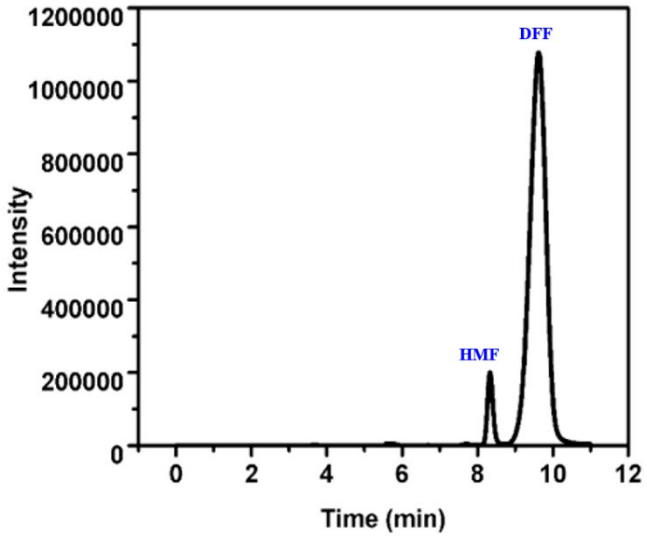

Figure S21. High performance liquid chromatograph (HPLC) spectrum of the reaction solution catalyzed by compound **1**. Reaction conditions: HMF (0.11 mmol), compound **1** (0.01 mmol), O_2 balloon, toluene (1 mL), naphthalene (48.8 μmol, internal standard), at 100 °C for 4 h.

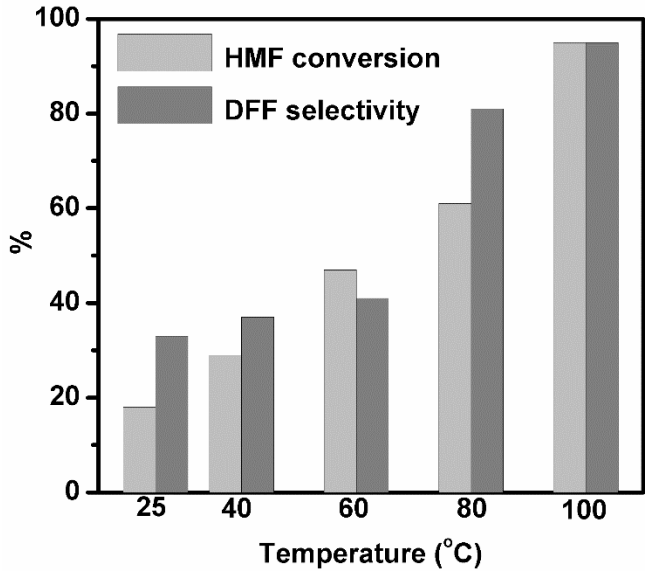

Figure S22. The effect of reaction temperature on the oxidation of HMF. Reaction conditions: HMF (0.11 mmol), compound **1** (0.01 mmol), O_2 balloon, toluene (1 mL), naphthalene (48.8 μmol, internal standard), at 100 °C for 4 h.

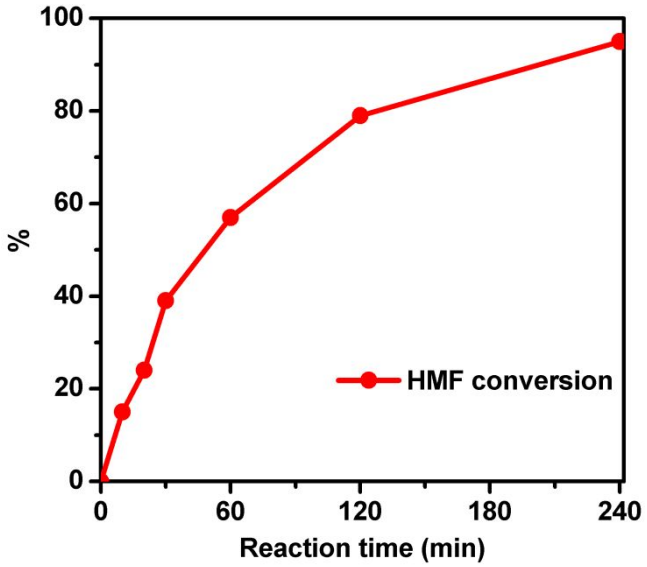

Figure S23. The effect of reaction time on the oxidation of HMF. Reaction conditions: HMF (0.11 mmol), compound **1** (0.01 mmol), O_2 balloon, toluene (1 mL), naphthalene (48.8 μmol, internal standard), at 100 °C for 4 h.

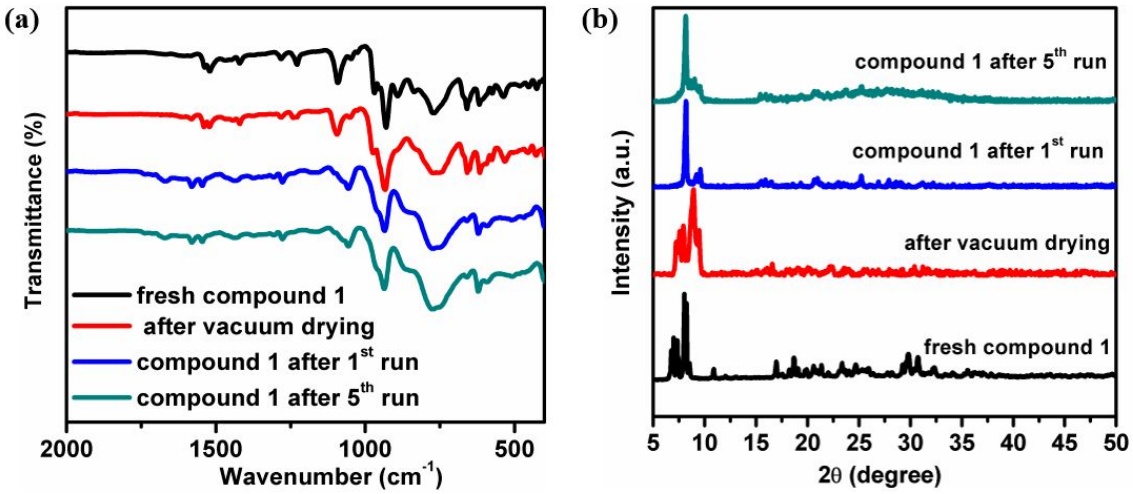

Figure S24. (a) The IR spectra of compound **1** before and after vacuum drying and recycle experiments (b) The XRD spectra of compound **1** before and after vacuum drying and recycle experiments. To evaluate the stability of compound **1** in the catalytic process, the FT-IR spectra and PXRD before and after vacuum drying and recycle test have been characterized and compared. The FT-IR spectra before and after the recycle test confirm the structural integrity of polyanion cluster, but the PXRD characteristic peaks of compound **1** changed obviously even after vacuum drying, indicating that the packing of POM cluster has changed. This phenomenon is often observed in POM compounds because the crystal packing of POM clusters would vary with the lose of the lattice water molecules and/or other solvent molecules.

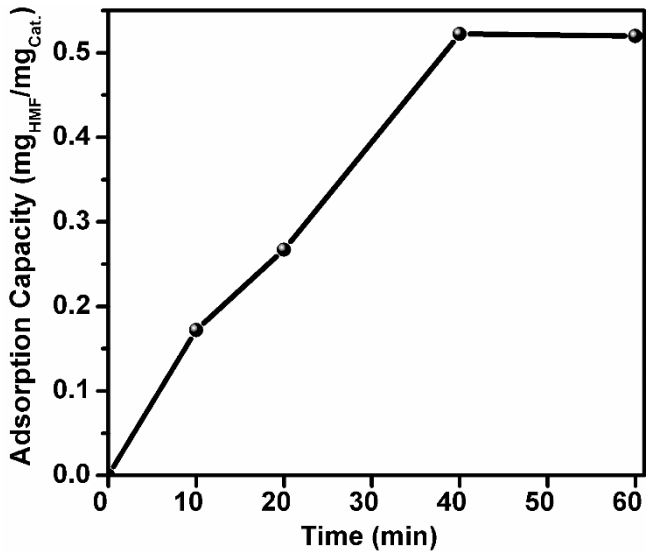

Figure S25. Adsorption capacity of compound **1** for HMF. Adsorption conditions: HMF (50 mg), compound **1** (40 mg), toluene (2 mL), naphthalene (48.8 μmol, internal standard) with stirring at room temperature.

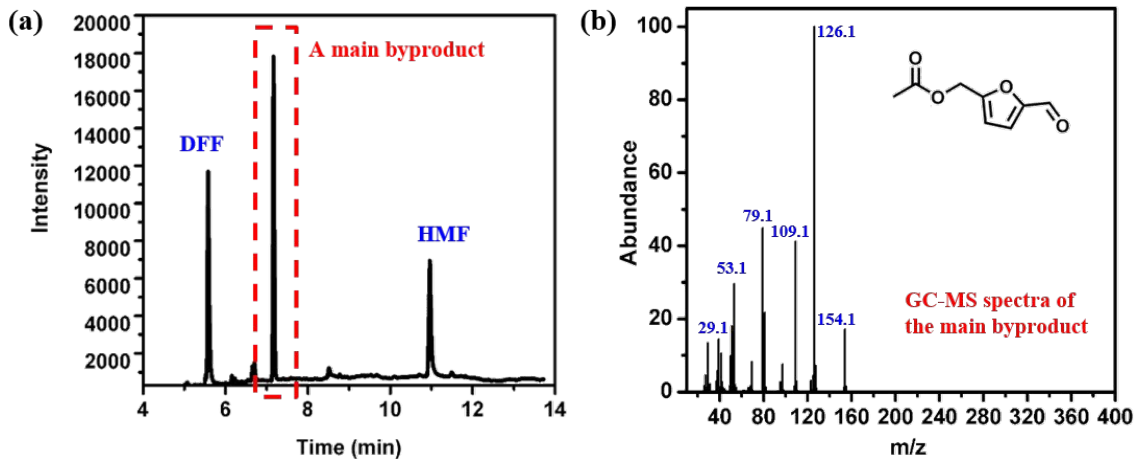

Figure S26. (a) GC spectrum of the reaction catalyzed by $H_5PMo_{10}V_2O_{40}$; (b) GC-MS spectrum of the main by-product. Reaction conditions: HMF (0.11 mmol), $H_5PMo_{10}V_2O_{40}$ (0.01 mmol), O_2 balloon, toluene (1 mL) at 100 ^oC for 4 h.

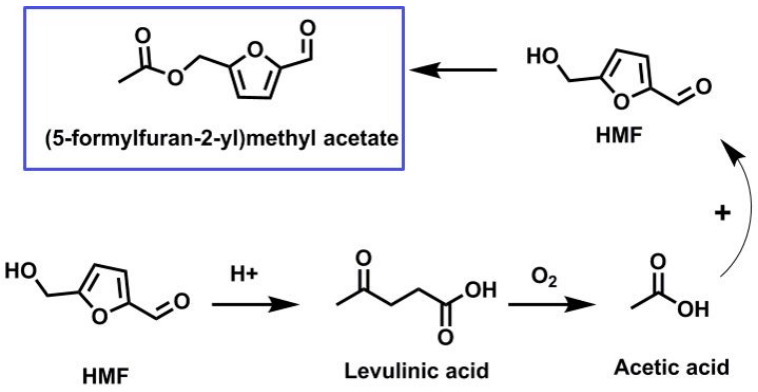

Figure S27 The formation of 5-acetoxymethyl-2-furcaldehyde.

Analysis of NMR

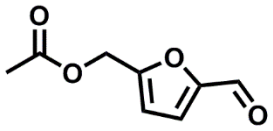

5-acetoxymethyl-2-furaldehyde, a main by-product in the oxidation of HMF catalyzed by $H_5PMo_{10}V_2O_{40}$**.**

^{1}H NMR (400 MHz, $CDCl_3$) δ = 9.64 (s, 1H), 7.21 (d, J = 3.6 Hz, 1H), 6.59 (d, J = 3.6 Hz, 1H), 5.12 (s, 2H), 2.1 (s, 3H).^{13}C NMR (101 MHz, $CDCl_3$) δ = 177.47, 169.97, 155.11, 152.55, 121.22, 112.21, 57.47, 20.33.

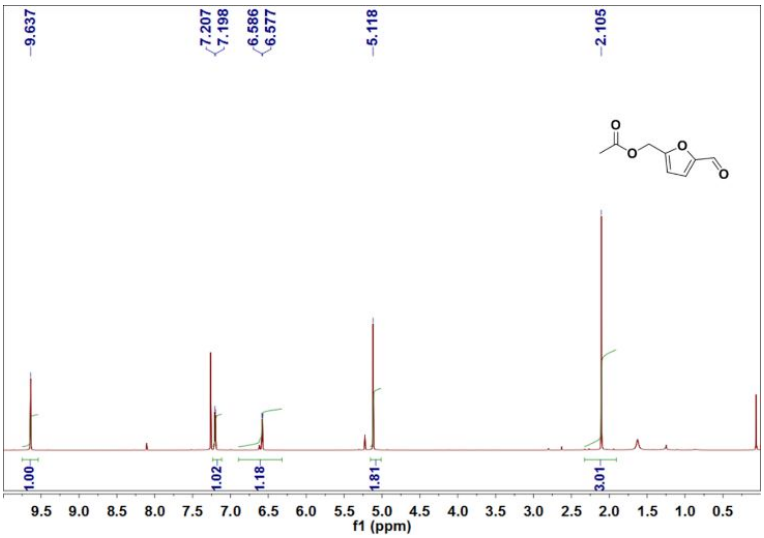

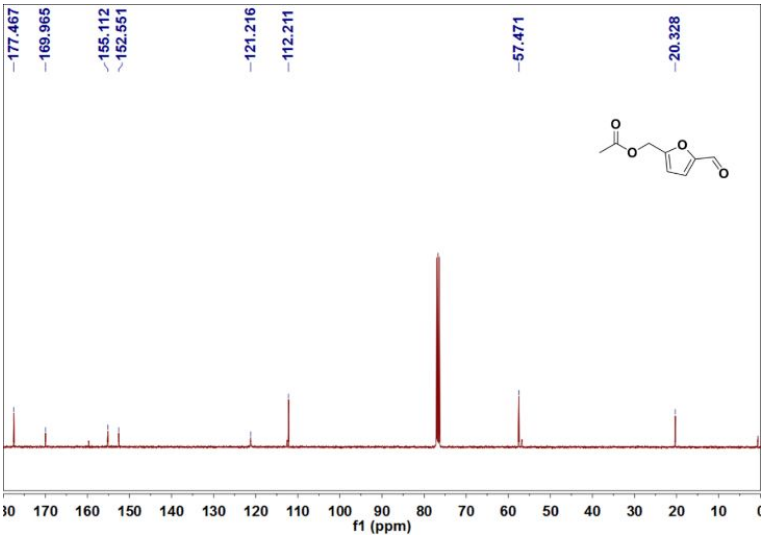
177.467
169.965
155.112
152.551
121.216
112.211
57.471
20.328
170 160 150 140 130 120 110 100 90 80 70 60 50 40 30 20 10
f1 (ppm)

Table S1. The selective oxidation of HMF to DFF by various catalysts.

Catalyst	Oxidant	Temp. (°C)	Time (h)	Conversion of HMF (%)	Selectivity of DFF (%)	Ref.
Heterogeneous catalysts						
Compound **1**	O_2 balloon	100	4	95	95	This work
Compound **2**	O_2 balloon	100	4	94	95	This work
Compound **3**	O_2 balloon	100	4	92	95	This work
$RuCo(OH)_2CeO_2$	0.1 MPa O_2,	120	12	96.5	86	1
Ru/CTF	2 MPa air	80	1	86.3	63.6	2
Fe_3O_4@SiO_2-NH_2-Ru(III)	0.1 MPa O_2	120	4	99.3	86.3	3
Cu-MnO_2	0.3 MPa O_2	140	5	86	96.1	4
Ag-OMS-2	1.5 MPa air	165	4	99	100	5
Fe_3O_4@SiO_2–NH_2–Cu^{2+}	0.28 MPa O_2	110	1	98.7	87.4	6
$Bi(NO_3)_3$-cellulose-CuNP	air	80	2	96.5	82	7
Fe_3O_4/Mn_3O_4	0.1 MPa O_2	120	4	99.8	82.1	8
V-Cu-CS	4 MPa air	140	4	>99	>98	9
V_2O_5/AC	0.28 MPa O_2	100	4	>95	>98	10
$VOPO_4$ $2H_2O$ (VOP)	0.1 MPa O_2	100	1	21	95	11
V_2O_5/zeolite	0.1 MPa O_2	125	3	84	99	12
CC-SO_3H-NH_2	0.1 MPa O_2	140	9	99	85	13
MOF-derived Fe–Co	1.0 MPa O_2	100	6	99	99	14
$ZnFe_{1.65}Ru_{0.35}O_4$	0.1 MPa O_2	110	4	100	93.5	15
OMS-2	0.5 MPa O_2	110	1	100	97.2	16
Ru-PVP/CNT	2 MPa O_2	120	12	>99	95	17
$Au_{0.5}Ru_{2.5}$/rGO	0.5 MPa O_2	80	8	95.7	90.9	18
V_2O_5@Cu-MOR	0.1 MPa O_2	120	7	>99.9	91.5	19
$H_5PMo_{10}V_2O_{40}/SiO_2$	1 MPa O_2	120	8	92.7	96	20
$H_5PMo_{10}V_2O_{40}$/chitosan	0.8 MPa O_2	120	6	96.2	97.8	21
Homogeneous catalysts						
GO+TEMPO	0.4 MPa O_2	100	6	100	99.5	22
CuCl /NCP	0.1 MPa air/O_2	RT	24	>95	>95	23
$VOSO_4$ /$Cu(NO_3)_2$	0.1 MPa O_2	80	1.5h	99	99	24
$Cu(NO_3)_2/VOSO_4$	0.1 MPa O_2	80	5	99	99	25
$Co(OAc)_2/Zn(OAc)_2/Br^-$	0.1 MPa O_2	90	4.5	100	96	26

Table S2. Information of the used chemicals.

Chemicals	Purity	Manufacturers
1,2,4-Trimethylbenzene	AR	Aladdin reagent Co., Ltd
1,4-Dichlorobutane	AR	ENERGY reagent Co., Ltd
Toluene	AR	ENERGY reagent Co., Ltd
5-Hydroxymethylfurfural	AR	Aladdin reagent Co., Ltd
Furan-2,5-dicarbaldehyde	AR	Aladdin reagent Co., Ltd
Ammonium metavanadate	AR	Aladdin reagent Co., Ltd
Vanadyl acetylacetonate	AR	Aladdin reagent Co., Ltd
Sodium Phosphate	AR	ENERGY reagent Co., Ltd
Sodium metavanadate	AR	Aladdin reagent Co., Ltd
Concentrated sulfuric acid	AR	ENERGY reagent Co., Ltd
1-Methylimidazole	AR	Aladdin reagent Co., Ltd
1-Ethylimidazole	AR	Aladdin reagent Co., Ltd
1-Propyl-1H-imidazole	AR	Aladdin reagent Co., Ltd
Phosphomolybdic Acid	AR	Aladdin reagent Co., Ltd
Cesium nitrate	AR	Aladdin reagent Co., Ltd
Ethyl acetate	AR	ENERGY reagent Co., Ltd
Naphthalene	AR	Aladdin reagent Co., Ltd

Table S3. Crystallographic data for compounds **1-3**.

Compounds	**1**	**2**	**3**
Formula	$C_{64}H_{105}N_{32}PMo_8V_8O_{48}$	$C_{85}H_{145}N_{34}PMo_8V_8O_{48}$	$C_{72}H_{121}N_{24}PMo_8V_8O_{44}$
*M*r	3296.73	3617.29	3232.89
Crystal system	triclinic	tetragonal	tetragonal
Space group	*P*-1	*P*4/n	*I*4/m
Temperature (K)	293(2)	293(2)	173(2)
a (Å)	14.9505(12)	14.8041(8)	15.2235(5)
b (Å)	15.4266(12)	14.8041(8)	15.2235(5)
c (Å)	25.628(2)	24.2594(14)	23.7613(14)
α (deg)	73.148(3)	90	90
β (deg)	73.203(2)	90	90
γ (deg)	65.305(2)	90	90
V (Å^3)	5042.9(7)	5316.7(7)	5506.8(5)
Z	2	2	2
*D*calc. (mg m^{-3})	2.129	2.059	2.182
F(000)	3216	3264	3624
GOOF	1.047	1.016	1.007
$R_1[I>2\sigma(I)]$[a]	0.0746	0.0867	0.0677
$wR_2[I>2\sigma(I)]$[b]	0.2249	0.2622	0.1762
*R*1(all data)[a]	0.0960	0.1518	0.1105
wR_2(all data)[b]	0.2489	0.3002	0.2167

[a]$R_1 = \Sigma(||F_0|-|Fc||)/\Sigma|F_0|$; [b]$wR_2=\Sigma[w(F_0^2-F_0^2)^2]/\Sigma[w(F_0^2)^2]^{1/2}$

Table S4. Bond Valence Sum calculations for compound 1.[27]

V site	BVS	Mo site	BVS
V1	4.457	Mo1	5.906
V2	4.464	Mo2	5.902
V3	4.459	Mo3	5.908
V4	4.471	Mo4	5.885
V5	4.516	Mo5	5.764
V6	3.984	Mo6	5.862
V7	4.512	Mo7	5.903
V8	3.975	Mo8	5.971

Table S5. Selected bond lengths [Å] and angles [deg] of compound **1-3**.

Compound **1**

Bond	**Å**	**Bond**	**Å**
V1-O19	1.928(7)	V2-O26	1.907(8)
V1-O24	1.909(8)	V2-O27	1.577(6)
V1-O25	1.578(6)	V2-O31	1.917 (7)
V1-O30	1.932(8)	V2-O38	1.922(8)
V1-O39	1.905(8)	V2-O33	1.931(7)
V1-O47	2.539(3)	V2-O48	2.481(3)
V5-O1	1.654(6)	V6-O12	1.592(6)
V5-O3	1.900(6)	V6-N2	2.120(9)
V5-O5	1.910(7)	V6-N5	2.114(8)
V5-O11	1.908(7)	V6-N1	2.111(8)
V5-O18	1.914(7)	V6-N9	2.106(8)
V6-O1	2.110(6)		
Angles	**deg**	**Angles**	**deg**
O25-V1-O24	102.2(4)	O27-V2-O38	100.4(4)
O24-V1-O30	158.0(3)	O31-V2-O38	90.3(3)
O30-V1-O45	63.9(4)	V5-O1-V6	178.7(4)
O25-V1-O19	101.1(3)	O1-V5-O3	115.0(3)
O39-V1-O30	86.7(3)	O1-V5-O5	112.8(3)
O25-V1-O30	99.8(4)	O3-V5-O11	80.8(3)
O25-V1-O45	158.6(4)	O3-V5-O5	132.2(3)
O39-V1-O45	65.4(4)	O1-V5-O18	113.5(3)
O24-V1-O45	94.9(4)	O3-V5-O18	80.7(3)
O19-V1-O45	92.5(4)	O11-V5-O18	133.7(3)
O31-V2-O33	157.9(3)	O5-V5-O18	80.9(3)
O26-V2-O33	88.4(3)	O12-V6-N1	93.9(3)
O38-V2-O33	86.0(3)	O12-V6-N9	94.4(3)
O27-V2-O31	101.3(3)	N1-V6-N9	88.8(3)
O31-V2-O26	86.8(3)	O12-V6-O1	178.4(3)

Compound **2**

Bond	**Å**	**Bond**	**Å**
V1-O11	1.65(2)	V1-O8(#3)	1.897(9)
V1-O8	1.897(9)	V4-N3	2.051(17)
V1-O8(#1)	1.897(9)	V4-O11	2.07(2)
V1-O8(#2)	1.897(9)	V4-O15	1.56(3)
Angles	**deg**	**Angles**	**deg**
V(1)-O(11)-V(4)	180	N(3)-V(4)-O(11)	85.4(5)
O(11)-V(1)-O(8)#3	112.6(3)	O(8)-V(1)-O(8)#3	134.8(6)
O(8)#2-V(1)-O(8)#3	81.5(2)		

#1 -y+3/2,x,z #2 y,-x+3/2,z #3 -x+3/2,-y+3/2,z

Compound **3**

Bond	**Å**	**Bond**	**Å**
V(1)-O(7)	1.903(7)	V(2)-O(8)	1.57(2)
V(1)-O(7)#1	1.903(7)	V(2)-N(1)	2.089(11)
V(1)-O(7)#2	1.903(7)	V(2)-O(4)	2.119(18)
V(1)-O(7)#3	1.903(7)		
Angles	**deg**	**Angles**	**deg**
O(7)#2-V(1)-O(7)#3	80.9(2)	N(1)-V(2)-O(4)	83.9(4)
O(7)-V(1)-O(7)#3	133.1(6)	O(8)-V(2)-N(1)	96.1(4)

#1 y, -x, z #2 -y, x, z #3 -x, -y, z

REFERENCES

(1) Wang, Y. M.; Liu, B.; Huang, K. C.; Zhang, Z. H. Aerobic Oxidation of Biomass-derived 5-(Hydroxymethyl)furfural into 2,5-Diformylfuran Catalyzed by the Trimetallic Mixed Oxide (Co–Ce–Ru). *Ind. Eng. Chem. Res*. **2016**, *53*, 1313–1319.

(2) Artz, J.; Mallmann, S.; Palkovits, R. Selective Aerobic Oxidation of HMF to 2,5-Diformylfuran on Covalent Triazine Frameworks-Supported Ru Catalysts. *Chemsuschem* **2015**, *8*, 672–679.

(3) Wang, S. G.; Zhang, Z. H.; Liu, B.; Li, J. L. Environmentally Friendly Oxidation of Biomass Derived 5-Hydroxymethylfurfural into 2,5-Diformylfuran Catalyzed by Magnetic Separation of Ruthenium Catalyst. *Ind. Eng. Chem. Res*. **2014**, *53*, 5820–5827.

(4) Tong, X. L.; Yu, L. H.; Chen H.; Zhuang, X. L.; Liao, S. Y.; Cui, H. G. Highly Efficient and Selective Oxidation of 5-Hydroxymethylfurfural by Molecular Oxygen in the Presence of Cu-MnO_2 Catalyst. *Catal. Commun*. **2017**, *90*, 91–94.

(5) Yadav, G. D.; Sharma, R. V. Biomass derived chemicals: Environmentally Benign Process for Oxidation of 5-Hydroxymethylfurfural to 2,5-Diformylfuran by using Nano-fibrous Ag-OMS-2-catalyst. *Appl. Catal., B* **2014**, *147*, 293–301.

(6) Liao, L. F.; Liu, Y.; Li, Z. Y.; Zhuang, J. P. Catalytic Aerobic Oxidation of 5-Hydroxymethylfurfural into 2,5-Diformylfuran over VO^{2+} and Cu^{2+} Immobilized on Amino-functionalized Core–shell Magnetic Fe_3O_4@SiO_2. *Rsc Adv*. **2016**, 6, 94976–94988.

(7) Baruah, D.; Hussain, F. L.; Suri, M.; Saikia, U. P.; Sengupta, P.; Dutta, D. K.; Konwar, D. Bi $(NO_3)_3 \cdot 5H_2O$ and Cellulose Mediated Cu-NPs-A Highly Efficient and Novel Catalytic System for

Aerobic Oxidation of Alcohols to Carbonyls and Synthesis of DFF from HMF. *Catal. Commun*. **2016**, *77*, 9–12.

(8) Liu, B.; Zhang, Z. H.; Lv, K. L.; Deng, K. J.; Duan, H. M. Efficient Aerobic Oxidation of Biomass-derived 5-Hydroxymethylfurfural to 2,5-Diformylfuran Catalyzed by Magnetic Nanoparticle Supported Manganese Oxide. *Appl. Catal., A* **2014**, *472*, 64–71.

(9) Le, N. T.; Lakshmanan, P.; Cho, K.; Han, Y. H.; Kim, H.. Selective Oxidation of 5-Hydroxymethyl-2-Furfural into 2,5-Diformylfuran over VO^{2+} and Cu^{2+} ions Immobilized on Sulfonated Carbon Catalysts. *Appl. Catal., A* **2013**, *464-465*, 305–312.

(10) Antonyraj, C. A.; Kim, B.; Kim, Y.; Shin, S.; Lee, K. Y.; Kim, I.; Cho, J. K. Heterogeneous Selective Oxidation of 5-Hydroxymethyl-2-Furfural (HMF) into 2,5-Diformylfuran Catalyzed by Vanadium Supported Activated Carbon in MIBK, Extracting Solvent for HMF. *Catal. Commun*. **2014**, *57*, 64–68.

(11) Carlini, C.; Patrono, P.; Galletti, A. M. R.; Sbrana, G.; Zima, V. Selective Oxidation of 5-Hydroxymethyl-2-furaldehyde to Furan-2,5-dicarboxaldehyde by Catalytic Systems Based on Vanadyl Phosphate. *Appl. Catal., A* **2005**, *289*, 197–204.

(12) Sádaba, I.; Gorbanev, Y. Y.; Kegnaes, S.; Putluru, S. S. R.; Berg, R. W.; Riisager A. Catalytic Performance of Zeolite-supported Vanadia in the Aerobic Oxidation of 5-Hydroxymethylfurfural to 2,5- Diformylfuran. *Chemcatchem* **2013**, *5*, 284–293.

(13) Rathod, P. V.; Nale, S. D.; Jadhav, V. H. Metal Free Acid Base Catalyst in the Selective Synthesis of 2,5-Diformylfuran from Hydroxymethylfurfural, Fructose, and Glucose. *ACS Sustainable Chem. Eng.* **2017**, *5*, 701–707.

(14) Fang, R , Luque, R , Li, Y . Selective Aerobic Oxidation of Biomass-derived HMF to 2,5-Diformylfuran using a MOF-derived Magnetic Hollow Fe-Co Nanocatalyst. *Green Chem*. **2016**, *18*, 3152–3157.

(15) Yang, Z. Z.; Qi, W.; Su, R. X.; He, Z. M. Selective Synthesis of 2,5-Diformylfuran and 2,5-Furandicarboxylic Acid from 5-Hydroxymethylfurfural and Fructose Catalyzed by Magnetically Separable Catalysts. *Energ. Fuel.* **2017**, *31*, 533–541.

(16) Nie, J. F.; Liu, H. C. Efficient Aerobic Oxidation of 5-Hydroxymethylfurfural to 2,5-Diformylfuran on Manganese Oxide Catalysts. *J. Catal.* 2014, *316*, 57–66.

(17) Chen, J. Z.; Zhong, J. W.; Guo, Y. Y.; Chen, L. M. Ruthenium Complex Immobilized on Poly(4-vinylpyridine)-functionalized Carbon-nanotube for Selective Aerobic Oxidation of 5-Hydroxymethylfurfural to 2,5-Diformylfuran. *Rsc Adv.* **2015**, *5*, 5933–5940.

(18) Červený, L.; Mikulcová, K.; Čejka, J. Shape-Selective Synthesis of 2-Acetylnaphthalene via Naphthalene Acylation with Acetic Anhydride over Large Pore Zeolites. *Appl. Catal., A* **2002**, *223*, 65–72.

(19) Zhang, W.; Xie, J. Y.; Hou, W.; Liu, Y. Q.; Zhou, Y.; Wang, J. One-Pot Template-Free Synthesis of Cu−MOR Zeolite toward Efficient Catalyst Support for Aerobic Oxidation of 5−

Hydroxymethylfurfural under Ambient Pressure. *ACS Appl. Mater. Interfaces* **2016**, *8*, 23122–23132.

(20) Yan, S. Q.; Li, Y.; Li, P. L.; Jia, T.; Wang, S. T.; Wang, X. H. Fabrication of Mesoporous POMs/SiO_2 Nanofibers through Electrospinning for Oxidative Conversion of Biomass by H_2O_2 and Oxygen. *RSC Adv.* **2018**, *8*, 3499–3511.

(21) Li, Y. M.; Li, P. L.; Cao, P.; Li, Y.; Wang, X. H.; Wang, S. T. Fabrication of Trifunctional Polyoxometalate−decorated Chitosan Nanofibers for Selective Production of 2,5−Diformylfuran. *ChemSusChem* **2020**, *13*, 5130–5131.

(22) Lv, G. Q.; Wang, H. L.; Yang, Y. X.; Deng, T. S.; Chen, C. M.; Zhu, Y. L.; Hou, X. L. Graphene Oxide: A Convenient Metal-free Carbocatalyst for Facilitating Aerobic Oxidation of 5‑Hydroxymethylfurfural into 2,5‑Diformylfuran. *ACS Catal.* **2015**, *5*, 5636–5646.

(23) Hansen, T. S.; Sádaba, I.; García-Suárez, E. J.; Riisage, A. Cu Catalyzed Oxidation of 5-Hydroxymethylfurfural to 2,5-Diformylfuran and 2,5-Furandicarboxylic Acid under Benign Reaction Conditions. *Appl. Catal. A* 2013, 456, 44–50.

(24) Jia, X. Q.; Ma, J. P.; Wang, M.; Du, Z. T.; Lu, F.; Wang, F.; Xu, J. Promoted Role of Cu(NO_3)$_2$ on Aerobic Oxidation of 5-Hydroxymethylfurfural to 2,5-Diformylfuran over $VOSO_4$. *Appl. Catal., A* **2014**, *48*, 231–236.

(25) Ma, J. P.; Du, Z. T.; Xu, J.; Chu, Q. H.; Pang, Y. Efficient Aerobic Oxidation of 5−Hydroxymethylfurfural to 2,5−Diformylfuran, and Synthesis of a Fluorescent Material. *ChemSusChem* **2011**, *4*, 51–54.

(26) Saha, B.; Dutta, S.; Abu-Omar, M. M. Aerobic Oxidation of 5-Hydroxylmethylfurfural with Homogeneous and Nanoparticulate Catalysts. *Catal. Sci. Technol.* **2012**, *2*, 79–81.

(27) Brese, N. E.; O'Keeffe M. *Acta Crystallogr. Sect. B* **1991**, *47*, 192–197.